Journal Pre-proof

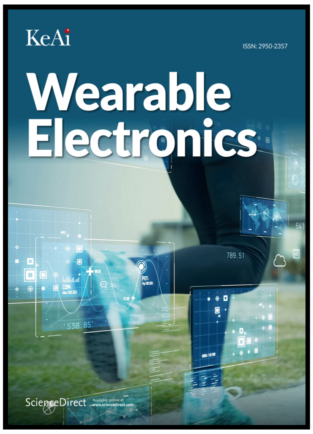

Hierarchical Carbon Nanotube-Decorated Polyacrylonitrile Smart Textiles for Wearable Biomonitoring

Junlong Huang, Yulin Cai, Guangzhong Xie, Xiangdong Xu, Zhenya Geng, Yadong Jiang, Yuanjie Su

PII: S2950-2357(24)00010-6

DOI: https://doi.org/10.1016/j.wees.2024.07.002

Reference: WEES10

To appear in: *Wearable Electronics*

Received date: 27 May 2024
Revised date: 27 June 2024
Accepted date: 21 July 2024

Please cite this article as: Junlong Huang, Yulin Cai, Guangzhong Xie, Xiangdong Xu, Zhenya Geng, Yadong Jiang and Yuanjie Su, Hierarchical Carbon Nanotube-Decorated Polyacrylonitrile Smart Textiles for Wearable Biomonitoring, *Wearable Electronics,* (2024) doi:https://doi.org/10.1016/j.wees.2024.07.002

Hierarchical Carbon Nanotube-Decorated Polyacrylonitrile Smart Textiles for Wearable Biomonitoring

Junlong Huang[1, †], Yulin Cai[1, †], Guangzhong Xie[1, *], Xiangdong Xu[1, *], Zhenya Geng[2, *], Yadong Jiang[1], Yuanjie Su[1, *]

[1] State Key Laboratory of Electronic Thin Films and Integrated Devices, School of Optoelectronic Science and Engineering, University of Electronic Science and Technology of China (UESTC), Chengdu 610054, China

[2] Department of Control Science and Engineering, Harbin Institute of Technology, Harbin 150001, China

* Corresponding Author: gzxie@uestc.edu.cn for Guangzhong Xie; xdxu@uestc.edu.cn for Xiangdong Xu; zhenya.geng@hit.edu.cn for Zhenya Geng; yjsu@uestc.edu.edu for Yuanjie Su. Yuanjie Su handle correspondence at all stages of refereeing and publication, also post-publication.

ABSTRACT: Respiration monitoring enables continuous assessment of physiological status and potential diseases. We reported a polyacrylonitrile/carbon nanotubes/latex composite membrane (PCM) capable of converting exhalation into a distinct current signal for respiratory rate and depth detection. The latex encapsulation design of respiratory sensor screens moist and thermal fluctuation of respiration and enables an accurate and reliable monitoring of exhaled gas flow. By modulating the compositional ratio, topological characters of interdigital electrode and aperture area, a rapid response time of 192 ms and recovery time of 104 ms, together with great fidelity and reliability were attained for discriminating breathing depth and rate. Combining with machine learning, versatile breathing patterns can be effectively discerned, achieving effective prognosis of respiratory diseases like diabetes, wheezing and obstructive sleep apnoea syndrome. This work endows a low-cost, efficient and stable route for sustainable wearable physiological assessment and disease recognition.

Graphical abstract

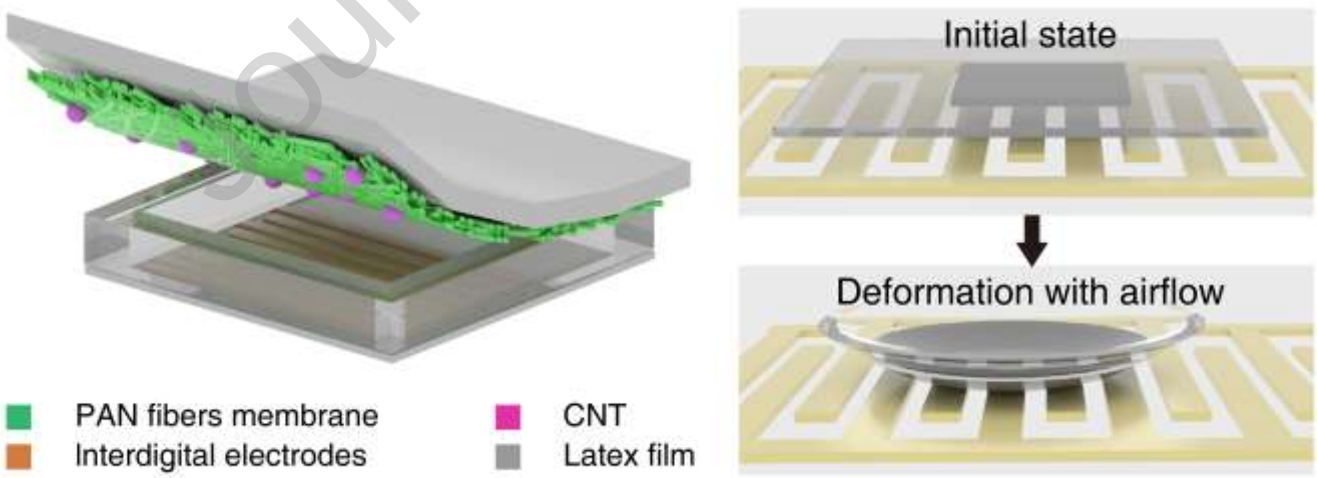

KEYWORDS: Respiratory sensor, hierarchical-structured, PAN/CNT composite membrane, physiological monitoring, machine learning

1. Introduction

Respiratory monitoring carries vital information about the breathing functionality and health status of the individual, accelerating early disease prognosis and physiological status acquisition [1-6]. The potential ramifications of not timely recognizing irregularities in respiratory characteristics can result in the escalation of negative health consequences, leading to increased risks and complications [7-9]. For instance, prolonged recurrent wheezing might cause pulmonary dysfunction and rise the risk of chronic obstructive pulmonary disease (COPD), pneumonia and asthma [10-11]. Sleep apnea not only reduces the quality of sleep and physical health, but also brings about neurological disorders, brainstem damage and congestive heart failure [12-16]. Additionally, deep and rapid breathing patterns (Kussmaul breathing) arising from euglycaemic diabetic ketoacidosis renders severe metabolic acidosis, which can also serve as an indicator of the prevalence of type 1 diabetes mellitus (T1DM) and type 2 diabetes mellitus (T2DM) [17-18]. However, in the absence of early detection and prompt interevent, prolonged and untreated symptom of hyperglycaemia gives rise to complications like cardiovascular disease, retinopathy, kidney disease and neuropathy. Due to intriguing merits of the portability and applicability, respiratory sensors enable continuous and reliable monitoring of respiration traits, achieving early recognition of potential diseases as well as prompt customized therapeutic regimen [19-22]. Nonetheless, the bulky, complicated and expensive sensing devices restrict the application of continuous on-body biomonitoring over a long periods of time [23-24]. As a consequence, a low-cost, widely-applicable, high-efficient respiratory sensor is desperately needed.

To date, existing wearable respiratory sensors fall into three categories according to the sensing mechanism: humidity sensitive mode [25-28], thermal sensitive mode [29-31] and pressure sensitive mode [32-37]. Among them, humidity sensitive mode respiratory sensors rely on the capacitance variation arising from the humidifying and dehumidifying associated with inhalation and exhalation of respiration; thermal sensitive mode respiratory sensors lie in the temperature fluctuation stemmed from periodic breathing behaviors. These two factors co-exist and interfere with each other, inevitably decaying the detection accuracy and stability [38-41]. Benefiting from its unique sensing principle, pressure sensitive mode sensors are insensitive to moist and thermal undulation in comparison with thermal and humidity modes counterparts, endowing fidelity and reliability for respiratory detection. One typical type of pressure sensitive mode respiratory sensors was enabled by evaluating expansion and contraction in the abdomen and chest, whereas body movement (e.g. limb motion or cough) easily gives rise to crosstalk signals [42]. Another type of pressure-mode respiratory sensors converts exhaled airflow into electric signal to eliminate the interference of limb movement. It is worth noting that a great deal of pressure mode respiratory sensors always relied on piezoelectric [43-45] and triboelectric effect [46-47], which cannot probe static gas flow rates and therefore fails to efficiently distinguish various breathing patterns [48-53]. To boost the accuracy in identifying inhalation and exhalation, Simran et al. developed a graphene/liquid elastic strain sensor integrated with a commercial mask to monitor respiratory airflow in real time through the deformation of the device under impact of respiratory airflow. However, this device suffers from severe baseline drift [42]. Therefore, a stable, reliable and accurate respiratory monitoring method is highly desired.

Herein, we reported a polyacrylonitrile/carbon nanotubes/latex composite membrane (PCM) based piezoresistive respiratory sensor. The PCM is constructed by combining PAN electrostatic spinning and CNT electrostatic spraying. By modulating the compositional ratio, topological characters of interdigital electrode and aperture area, a rapid response time of 192 ms and recovery time of 104 ms, together with great fidelity and reliability were attained for discriminating breathing depth and rate. Assisted by machine learning, PCM enabled sensors are capable of identifying versatile breathing patterns including 'normal, deep and rapid' and 'Kussmaul Breath', and discerning respiratory diseases like diabetes, wheeze and obstructive sleep apnoea syndrome (OSAS). This work opens up a new paradigm for developing respiratory sensors with low cost, rapid and stable wearable bioelectronics in the field of noninvasive physiological biomonitoring.

2. Experimental section

2.1 Materials

The Multi-walled carbon nanotube DMF dispersion (1.5 wt%) was purchased from Chengdu Organic Chemistry Co., Ltd. (China). The PAN (25014-41-9) was purchased from Wuhan Kermit Biomedical Technology Co., Ltd. (China). N, N- dimethylformamide (DMF), acetone, and nanosilver conductive ink (N196405) were purchased from Aladdin (Shanghai, China). Mechanical anemometer and hairdryer purchased from BOE. All the chemicals were used as received without further purification.

2.2 Fabrication of PAN/CNT composite membrane

The parameters of electrostatic spraying of multi-walled carbon nanotubes DMF dispersion were as follows: the working voltage was 18 kV, the speed of the injection pump was set to 2 μL/min, 4 μL/min and 6 μL/min, respectively. The distance between the collecting devices (aluminium foil on rollers) and the needle was 10 cm, and the electrostatic spraying time was 2 h. The electrospinning solution was prepared by adding 1 g of PAN to a mixed solution of 3 mL of actone and 7 mL of DMF, followed by magnetic stirring at 60 °C for 4 hours. The electrospinning parameters of PAN nanofibre membranes were as follows: the working voltage was 18 kV, the speed of the injection pump was 5 μL/min. The distance between the collecting devices (aluminium foil on rollers) and the needle was 10 cm, and the electrospinning time was 2 h. Electrostatic spraying and spinning at the same time, spraying and spinning needles are 10 cm apart.

2.3 Device fabrication

Interdigital electrodes were screen printed onto a plastic substrate and then the hollow structure of the plastic was fixed over the interdigital electrodes with adhesive. The colloidal dispersion was sprayed onto an ultra-thin latex film and then the PAN/CNT composite membrane was bonded to the latex film. The latex film was secured over the hollow structure of the plastic with adhesive tape so that the PCM was suspended above the interdigital electrode.

2.4 Characterization and measurement

The morphology of the PAN/CNT composite membranes was obtained by scanning electron microscopy (SEM, Inspect F50, FEI, USA), and the elemental content analysis of the PCM was analysed by SEM and Fourier transform infrared spectroscopy (FTIR, Nicolet 6700, Thermo Fisher, USA). The hairdryer was switched on and the maximum wind speed generated by the hairdryer was measured by an anemometer to be 14m/s (Fig. s4). The air speed is adjusted by adjusting the distance between the hairdryer and the sensor, using an anemometer to determine the exact distance. The electromechanical response of the sensor was measured by a Keithley 4200 SCS semiconductor parameter analyzer. The current measured at 1 m/s was used as the initial current I_0, and the sensitivity formula being expressed as $S= (I-I_0)/ I_0\Delta v$.

3. Results and discussion

3.1 Sensor structure

Figure 1a elucidates the synthesis process of PCM based respiratory sensor by coupling electrospinning and electrostatic spraying, endowing excellent mechanical robustness and great piezoresistive characters for real-time respiration monitoring. In comparison to the spinning membranes impregnated with conductive materials, the combination between electrostatic spinning of hierarchical substrate and electrostatic spraying of conductive materials results in a more homogeneous and repeatable composite membrane. The low-density, porous and three-dimensional interconnective flexible PAN electrospun fiber membranes are responsible for durability and stretchability under exhaled airflow [54-55]. Incorporation of high-conductive, low-density carbon nanotubes (CNTs) into electrospun PAN scaffold establishes conducting pathway for enabling piezoresistive perception without scarifying the mechanical properties [56-58]. Due to the intrinsic hydrophobicity and good flexibility, encapsulation of the PAN/CNT membranes using latex film eludes moisture interference originating from exhaled gases (Fig. 1b), enabling an accurate and reliable monitoring of exhaled gas flow in terms of mechanical deformation. This device configuration design guarantees the sensitivity and stability of the PCM based respiratory sensors (Fig. 1c).

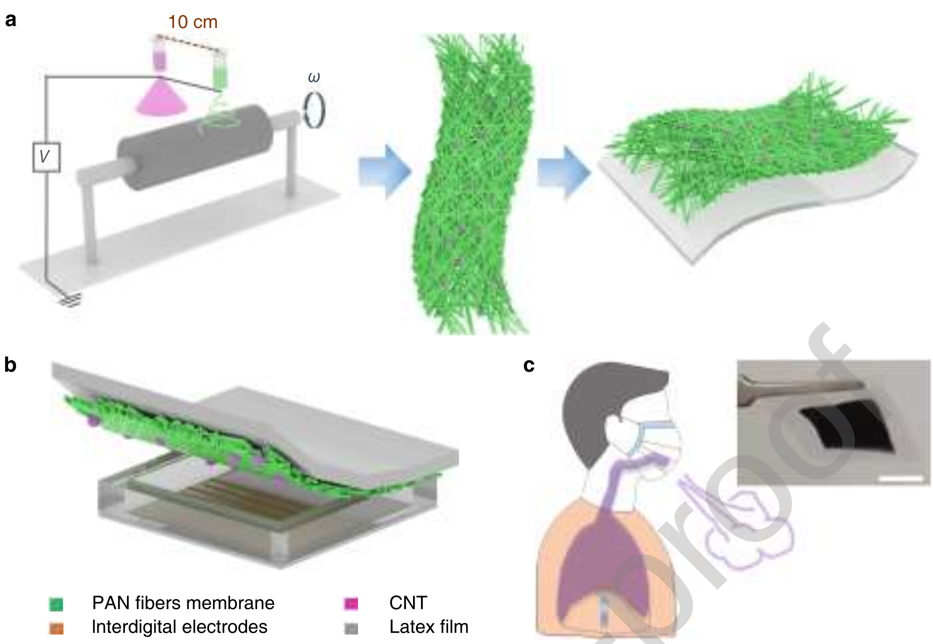

Figure 1. The fabrication process of the polyacrylonitrile/carbon nanotubes/latex composite membrane (PCM) based exhalation flow sensor and application sketch. (a) PCM preparation procedure. (b) Sensor structure. (c) Expiratory test.

3.2 Morphological and elemental analyses

To unravel the morphology of PCM based respiratory sensors, scanning electron microscope (SEM) was employed to characterize the as-electrospun PAN/CNT composite membranes. As shown in Fig. 2a, the randomly distributed pores impart sufficient surficial area and adsorbed sites for decoration of conducting fillers. Moreover, modulation of electrostatic spinning rate of PAN as well as electrostatic spraying rate of CNT varies the topological structure of hierarchical PCM films (Figs. 2b-d). It can be clearly seen that the CNTs gradually agglomeratea on the hierarchical scaffold of as-prepared PAN textile with increasing electrostatic spraying rate (Figs. 2b-e). The homogeneity of the PAN/CNT composite membrane implies the successful inclusion of CNTs as the conducting fillers as displayed in the enlarged section of Figure 2e. To investigate the compositional properties of the prepared PCMs doped with various CNT concentration, Energy Dispersive Spectroscopy (EDS) and Fourier Transform Infrared Spectroscopy (FTIR) spectroscopy were performed as shown in Figures 2f-i. Clearly, the density of nitrogen gradually dilutes with increasing electrostatic spraying rates of 0, 2, 4 and 6 µl/min (Fig. 2f). The EDS results show that the density of carbon is proportional to CNT doping amount, in which the specific mass ratio of carbon to nitrogen increases from 70.1:29.9 to 78.04:21.96 (Fig. 2g，Fig. 2h and Tab. S1) [59-60]. According to the FTIR results, the characteristic peaks at 2926, 2244 and 1452 cm^{-1} are attributed to the stretching vibration of the -C-H bonds, the -C-N bonds and the bending vibration of the -C-H bonds, respectively [61-62]. Strikingly, the penetration of CNT into the electrospun PAN fibers dramatically decay the reflectance of PCMs owing to the strong light absorption of CNT fillers (Fig. 2i). Furthermore, absorption peaks of C=C bonds at 1647 cm^{-1} were observed in all the PCMs, indicating successful loading of CNT via electrostatic spraying [63].

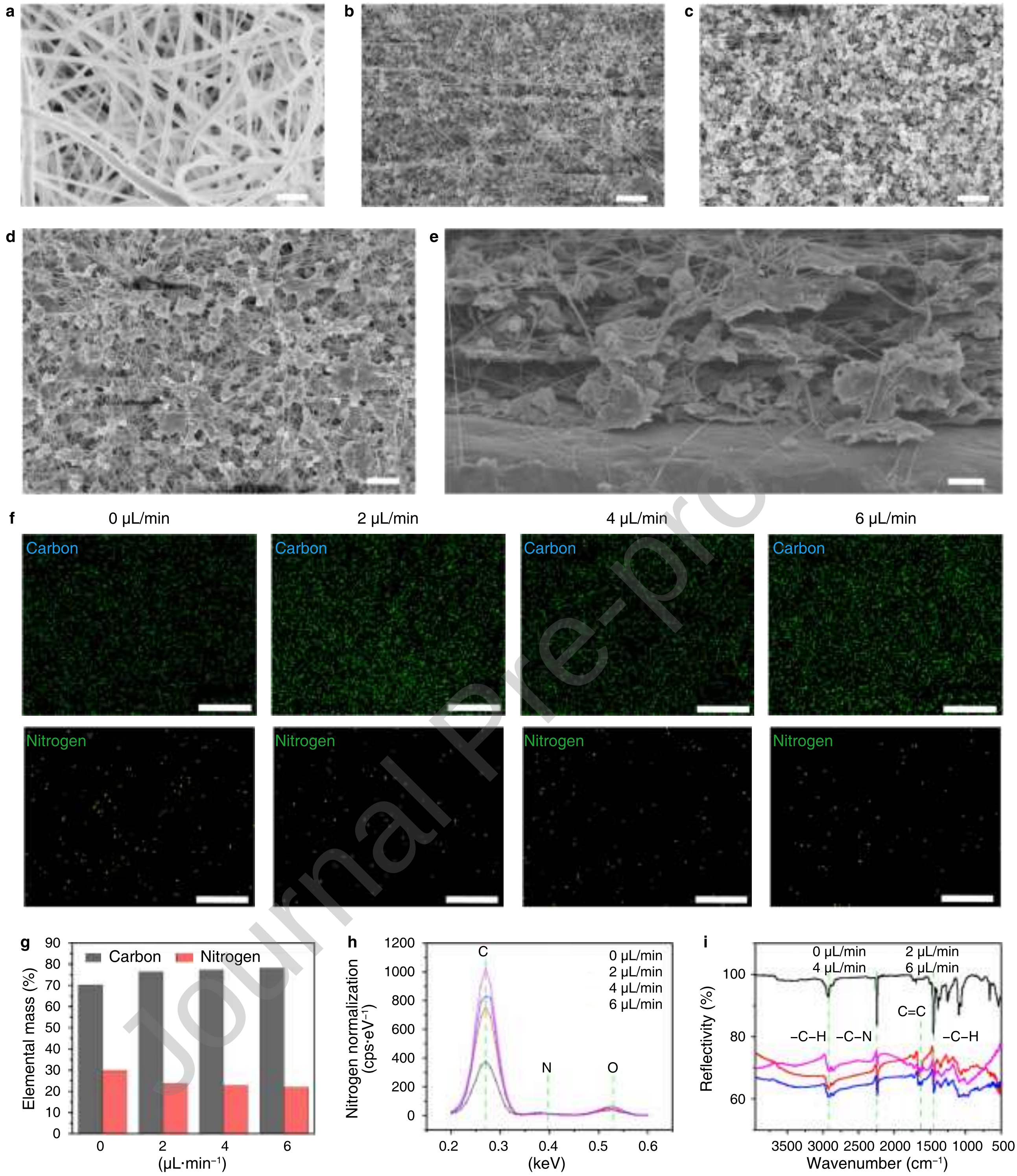

Figure 2. Characterisation of PCMs. (a) Scanning electron microscope (SEM) image of PAN spun membrane with an electrostatic spinning rate of 5 μL/min. (b-d) SEM image of PCMs synthesized with an electrostatic spinning rate of 5 μL/min and an electrostatic spraying rate of 2 μL/min (b), 4 μL/min (c), 6 μL/min (d). (e) Cross-section of PCM in (d). (f) Elemental carbon and nitrogen scans were performed on PCMs prepared at electrostatic spraying rates of 0, 2, 4 and 6 μl/min. (g) Mass ratios of carbon to nitrogen for PCMs produced at electrostatic spray rates of 0, 2, 4 and 6 μl/min. (h) EDS mapping of PCMs fabricated with an electrostatic spraying rate of 0, 2, 4 and 6 μL/min. (i) FTIR of PCMs fabricated with an electrostatic spraying rate of 0, 2, 4 and 6 μL/min.

3.3 Sensing mechanism

Figure 3a and 3b elucidate the sensing mechanism of as-prepared PCMs based respiratory sensor. Under the initial status without exhalation, a constant gap distance between PCM and the interdigital electrodes blocks the transportation of conducting carriers (Fig. 3a). Therefore, no current was detected in the initial state. Once exhalation occurs, the exhaled gas compresses the distance and forms conducting routes between PCM and the interdigital electrodes (Fig. 3b). The increasing exhalation flow rate continuously shrinks the gap distance, achieving a larger contact area and thus greater conducting current (Fig. 3c). Under relative low expiratory flow, the device resistance is dominated by contact area between the hierarchical PCMs and interdigital electrodes. Whilst, under high breathing flow, the device resistance is mainly relied on the contacting area among doped CNT fillers (Fig. 3d) [64-65].

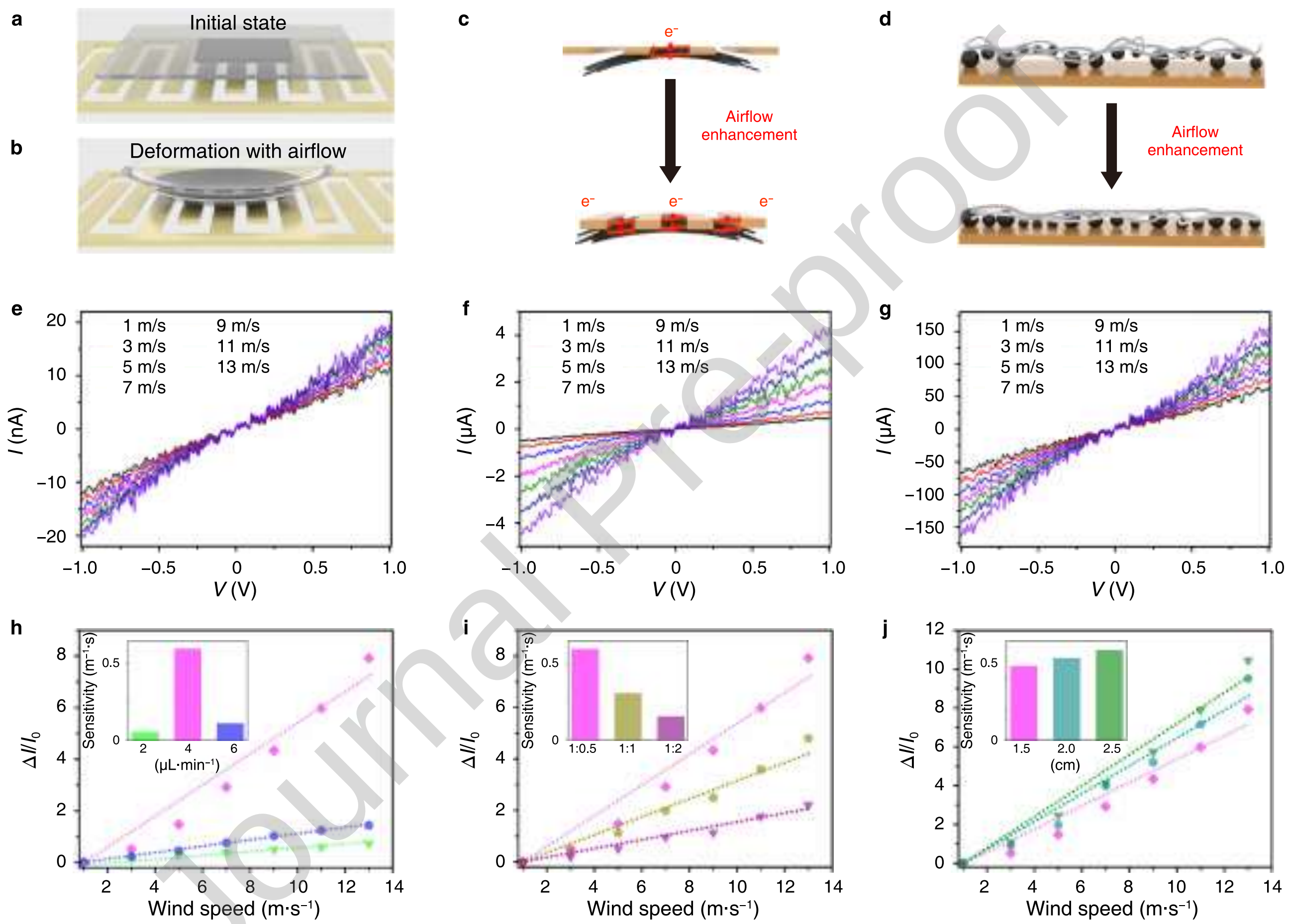

Figure 3. Sensitive mechanisms and performance of devices. (a) Initial state of the device. (b) Deformation of PCM of the device. (c) The increased contact of the PCM with the interdigital electrode improves sensor response as airflow increases. (d) Hierarchical structure on the surface of the PAN/CNT membrane improves the response of the sensor as the airflow increases. (e-g) I-V curves of sensors at different pressures with an electrostatic spraying rate of 2 μL/min (e), 4 μL/min (f), and 6 μL/min (g). (h) Sensor performance for electrostatic spraying rates of 2, 4, and 6 μL/min at different airflow rates. (i) Performance of sensors with different width-to-spacing at different airflow rates. (j) Performance of sensors with different opening size at different airflow rates.

To explore the sensing performance of the PCM-based respiratory sensors with various compositional ratios, we characterize the output current of fabricated sensors in response to diverse exhaled flow (Figs. 3e-g). Notably, all PCMs exhibit good ohmic contacts, where the initial resistance is reversely proportional to CNT concentration. Apparently, the pressure sensors synthesized with an electrostatic spraying rate of 4 μL/min demonstrate superior sensitivity in comparison with other versions (Fig. 3h). This is because that the sparse CNTs cannot build up compact piezoresistive conducting network (Fig. 2b) while the excessive CNTs screen the relative resistance change under a constant applied force (Figs. 2d and e). To ensure the optimal sensing performance, the following measurement was conducted using the sensor based with an electrostatic spraying rate of 4 μL/min.

Figure 3i and Figure s2 shows the dependence of sensing response of PCM-based devices on the width-to-spacing ratio of interdigital electrode. It can be clearly seen that the augmented width-to-spacing ratio gradually up-regulates the sensitivity of the device. This tendency can be explained by the fact that enhancement of the spacing between the interdigital electrodes is detrimental to the formation of a conductive path, which considerably reduces the carrier transportation between the electrodes and the PCMs. Additionally, the influence of plastic sheet opening areas on the sensing performance of PCM-based sensors was uncovered in Figure 3j and Figure s3. It is worth noting that a slight increase in sensitivity stemmed from an expanded opening area, which in turn resulted in a reduction in miniaturization and portability. To ensure the portability of the respiratory sensor, the following tests were conducted via an opening area of 1.5 cm x 1.5 cm.

3.4 Device Perfomance

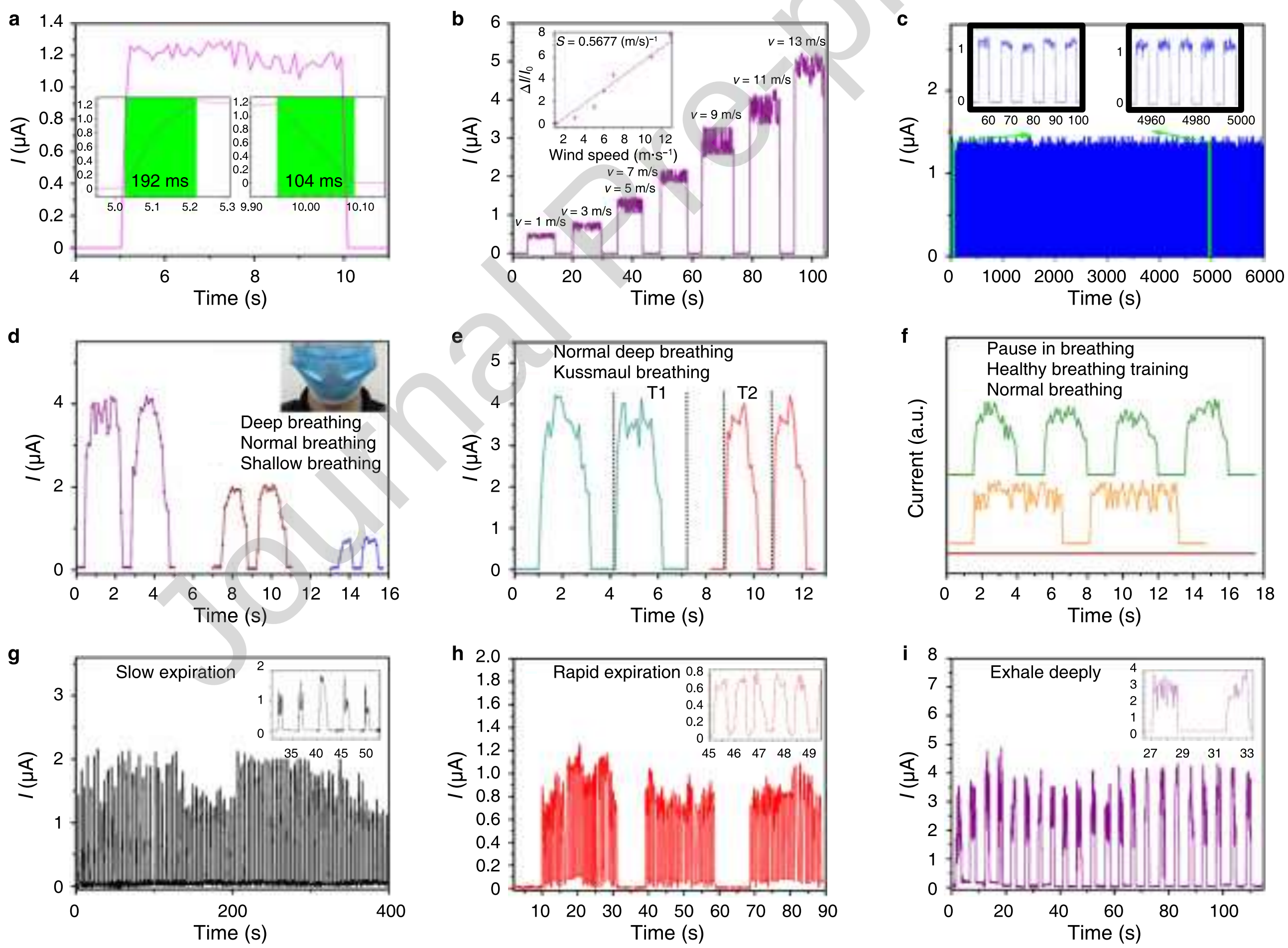

Figure 4. Performance of the device. (a) Response time and recovery time of the device under the flow rate of 5 m/s. (b) Device response to varying airflows. (c) Repeatability of device response at 5m/s airflow. (d) The ability of the device to discriminate the intensity of respiration. (e) The ability of the device to discriminate between respiratory frequencies. (f) The ability of the device to discriminate between respiratory rhythms. (g) Real-time response of the device to slow expiration. (h) Real-time response of the

device to rapid expiration. (i) Real-time response of the device to deep exhalation.

Figure 4a elucidates the dynamic response of PCM enabled respiratory sensor under impact of exhaled gas flow, where a response time of 193 ms and recovery time of 104 ms was observed, respectively. The rapid response behaviors assure the device to discriminate the real-time breathing characteristics even under rapid respiratory pattern (Fig. 4a). A linear relationship between output current and airflow velocity corroborates the great capability in distinguishing the respiratory traits (Fig. 4b). Moreover, unnoticeable attenuation and distortion of output signals were detected after 600 cycles of loading and unloading of 5 m/s breathing flow, implying the durability and reliability (Fig. 4c). To verify the competence for respiratory monitoring, the PCM based sensor was mounted on a wearable mask to capture the real-time output signal profiles for deep, normal, shallow breathing patterns (Fig. 4d). Note that the respiratory rate and depth can be respectively associated with interval and peak-to-peak intensity of signal waveforms. Evidently, a deep breathing pattern contributes to a larger interval and huger peak-to-peak intensity. As a consequence, the as-prepared PCM based sensor can not only discern breathing rhythms such as normal breathing, deep breathing, kussmaul breathing, pause in breathing, etc., but also identify respiratory dynamics under physiological training (Figs. 4e and 4f) [66-68]. Figures 4g-i display the real-time waveforms towards slow expiration, rapid expiration and deep exhalation. Among these three different simulated respiratory patterns, the intensity and interval of the signal varies distinctly with other versions, confirming capability in discriminating respiratory characteristic.

3.5 Machine learning and applications

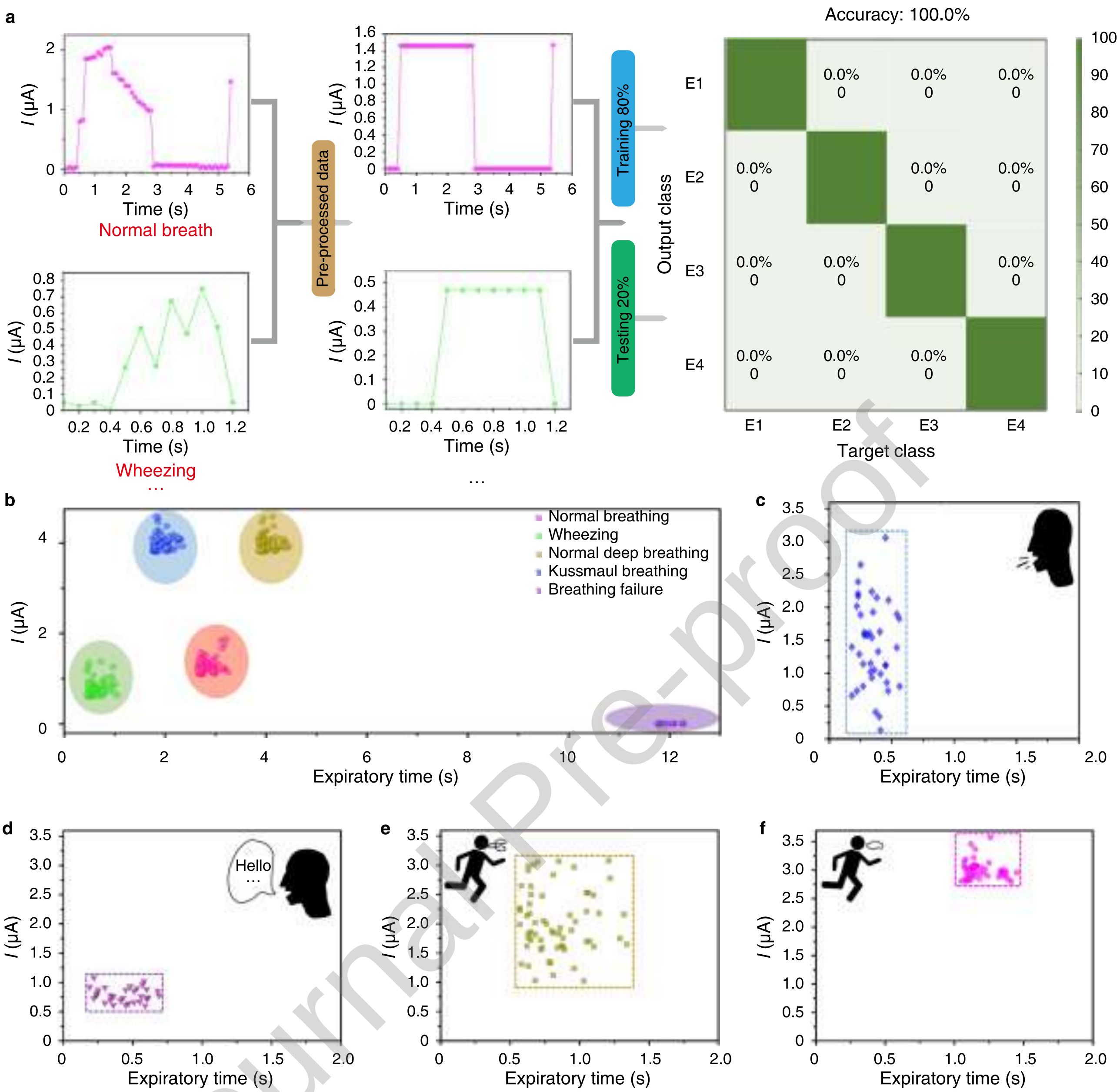

Figure 5. Application of the device based on machine learning. (a) Flowchart of machine learning. (b) Classification of respiratory characteristics and possible causes of these respiratory characteristics. (c) Cough monitoring (per minute). (d) Speaking monitoring (per minute). (e) Irregular breathing while running (per minute). (f) Regular breathing while running (per minute).

Failure in perceiving respiratory abnormalities gives rise to complications like diabetes mellitus, hyperglycaemia, cardiovascular disease and retinopathy. To boost the accuracy and fidelity in identifying respiratory traits, machine learning (ML) was adopted to analyze the acquired sensing signals and predict the potential diseases (Fig. 5a). Firstly, the large amount of raw time series data collected by the sensor was normalized before delivery to ML algorithms. Subsequently, the dataset was pre-processed in sequence by data cleaning, data organisation and feature extraction. Then, identification of respiratory patterns was realized by predicting the value of a new dataset accordingly. It is worth mentioning that, due to fluctuations in the signal, the data needs to be pre-processed and then fed to train a 1D CNN model. Data sets were created from four breathing patterns (normal breathing, wheezing, breathing failure, and kussmaul breathing). For each breathing pattern, the entire data was divided into a training set (80%) and a testing set (20%). Notably, various breathing patterns feature with diverse regions of respiratory rate and respiratory intensity were labeled in Figure 5b. Considering the constant oxygen consumption rate during static physiological state (e.g. sitting and driving), the duration of breathing is reversely proportional to the intensity of breathing. To this end, an obvious increased intensity of breathing with a fixed or even shorter duration implies a potential illness such as diabetes mellitus and pulmonary dysfunction. Wheezing causes a dramatic reduction in breathing time and apnoea renders a large interval between two cycles, which can be clearly differentiated in the time span axis (Fig. 5b).

Nonetheless, discrimination of individual breath traces (depth and rate) does not means accurate identification of the potential respiratory diseases. This is because that the respiratory features of wheezing, speaking and light coughing are quite similar. To further identify predisposing factors for respiratory characteristics, an integration of respiratory characteristics over a period of time is demanded. Figures 5c and 5d reveal the respiratory characteristics extracted from a one-minute duration of coughing and talking, respectively. Significantly, they have a large overlap and it is impossible to distinguish between a light cough and speech. Evidently, acute cough can be clearly distinguished because of the abrupt increase in respiratory intensity, which can be used as an early warning of aggravation for coughing patients. Furthermore, the ML assisted respiratory monitoring can be implemented to direct the physical training. Amateurish runners deliver irregular and unstable respiratory rate and depth during running, which contributes to a relative large variation range in breathing intensity and duration (Fig. 5e). In contrast, a small variation range in breathing intensity and duration was observed from a regular exercise running person (Fig. 5f), indicating the practicability of PCMs in guidance and feedback of physiological training. In addition to respiratory monitoring, the sensor is capable of detecting wind speed through the recognition of real-time output current, making it an ideal solution for a wide range of applications, including weather monitoring, marine surveillance, agricultural management and so on.

4. Conclusions

We constructed a PCM-based respiratory sensor by combining electrospinning and electrostatic spraying. By modulating CNT loading amount, width-to-spacing ratio of the interdigital electrode, and aperture areas, a fast response time of 192ms and recovery time of 104ms, a sensitivity of 0.5677 $(m/s)^{-1}$ were attained, enabling accurate detection of respiratory behaviors. The implementation of high-sensitive respiratory sensors can facilitate the acquisition of more detailed data, thereby enabling the refinement of respiratory patterns. Accordingly, the device sensitivity should be augmented in future iterations to achieve enhanced performance. With the assistant of machine learning, versatile breathing modes as well as potential diseases can be efficiently identified. This work provides a new possibility for developing soft bioelectronics for wearable physiological monitoring and disease prognosis.

Funding
This work was partially supported by the National Natural Science Foundation of China (grant no. 62074027).

Author Contributions

Conceptualization, Y. S. and G. X.; investigation, J. H. and X. X.; Writing – original draft, J. H. and Z. G.; Writing – review & editing, J. H., Y. C. and Y. S.; Supervision, Y. S. and G.X.; Funding acquisition, Y.S.

Declaration of Competing Interest

The authors declare no conflict of interest.

References

[1] Z. Yin, Y. Yang, C. Hu, J. Li, B. Qin, X. Yang, Wearable respiratory sensors for health monitoring. NPG Asia Mater. 16 (2024) 1-29.

[2] T.L. Mathew, P. Pownraj, S. Abdulla, B. Pullithadathil, Technologies for Clinical Diagnosis Using Expired Human Breath Analysis. Diagnostics 5 (2015) 27-60.
[3] Y. Khan, A. E. Ostfeld, C. M. Lochner, A. Pierre, A. C. Arias, Monitoring of vital signs with flexible and wearable medical devices. Adv. Mater. 28 (2016) 4373–4395.
[4] Y. Su, G. Chen, C. Chen, Q. Gong, G. Xie, M. Yao, J. Chen, Self-powered respiration monitoring enabled by a triboelectric nanogenerator. Adv. Mater. 33 (2021) 2101262.
[5] Y. Su, Y. Liu, W. Li, X. Xiao, C. Chen, H. Lu, J. Chen, Sensing–transducing coupled piezoelectric textiles for self-powered humidity detection and wearable biomonitoring. Mater. Horiz. 10 (2023) 842-851.
[6] Y. Li, W. Li, Z. Jin, X. Luo, G. Xie, H. Tai, Y. Su, Ternary ordered assembled piezoelectric composite for self-powered ammonia detection. Nano Energy 122 (2024) 109291.
[7] S. Shen, Q. Zhou, G. Chen, Y. Fang, O. Kurilova, Z. Liu, J. Chen, Advances in wearable respiration sensors. Mater. Today (2024).
[8] W. Kwak, J. Yin, S. Wang, J. Chen, Advances in triboelectric nanogenerators for self-powered wearable respiratory monitoring. FlexMat 1 (2024) 5-22.
[9] A. Libanori, G. Chen, X. Zhao, Y. Zhou, J. Chen, Smart textiles for personalized healthcare. Nat. Electron. 5 (2022) 142-156.
[10] T. Jartti, J. E. Gern, Role of viral infections in the development and exacerbation of asthma in children. J ALLERGY CLIN IMMUN 140 (2017) 895-906.
[11] H. Ma, Y. Li, L. Tang, X. Peng, L. Jiang, J. Wan, F. Suo, G. Zhang, Z. L. C. Luo, Impact of childhood wheezing on lung function in adulthood: A meta-analysis. PloS one 13 (2018) e0192390-e0192390.
[12] F. Mendonça, S. S. Mostafa, A. G. Ravelo-García, F. Morgado-Dias, T. Penzel, Devices for home detection of obstructive sleep apnea: A review. SLEEP MED REV 41 (2018) 149-160.
[13] A. Malhotra, R. L. Owens, What is central sleep apnea? RESP CARE 55 (2010) 1168-1178.
[14] Y. Su, C. Chen, H. Pan, Y. Yang, G. Chen, X. Zhao, J. Chen, Muscle fibers inspired high-performance piezoelectric textiles for wearable physiological monitoring. Adv. Funct. Mater. 31 (2021) 2010962.
[15] Y. Su, W. Li, L. Yuan, C. Chen, H. Pan, G. Xie, J. Chen, Piezoelectric fiber composites with polydopamine interfacial layer for self-powered wearable biomonitoring. Nano Energy 89 (2021) 106321.
[16] Y. Su, L W. i, X. Cheng, Y. Zhou, S. Yang, X. Zhang, J. Chen, High-performance piezoelectric composites via β phase programming. Nat. Commun. 13 (2022) 4867.
[17] A. L. Peters, E. O. Buschur, J. B. Buse, P. Cohan, J. C. Diner, I. B. Hirsch, Euglycemic Diabetic Ketoacidosis: A Potential Complication of Treatment with Sodium-Glucose Cotransporter 2 Inhibition. DIABETES CARE 38 (2015) 1687-93.
[18] B. Long, S. Lentz, A. Koyfman, M. Gottlieb, Euglycemic diabetic ketoacidosis: etiologies, evaluation, and management. AM J EMERG MED 44 (2021) 157-160.
[19] Y. Su, J. Wang, B. Wang, T. Yang, B. Yang, G. Xie, J. Chen, Alveolus-inspired active membrane sensors for self-powered wearable chemical sensing and breath analysis. ACS nano 14 (2020) 6067-6075.
[20] Y. Su, T. Yang, X. Zhao, Z. Cai, G. Chen, M. Yao, J. Chen, A wireless energy transmission enabled wearable active acetone biosensor for non-invasive prediabetes diagnosis. Nano Energy 74 (2020) 104941.
[21] C. Chen, G. Xie, J. Dai, W. Li, Y. Cai, J. Li, Y. Su, Integrated core-shell structured smart textiles for active NO2 concentration and pressure monitoring. Nano Energy 116 (2023) 108788.
[22] Y. Su, S. Chen, B. Liu, H. Lu, X. Luo, C. Chen, Y. Jiang, Maxwell displacement current induced wireless self-powered gas sensor array. Mater. Today Phys. 30 (2023) 100951.
[23] Q. Pan, B. Damien, C. Eric, Current status and future challenges of sleep monitoring systems: Systematic review. JMIR Biomedical Engineering 5 (2020) e20921.
[24] T. L. Mathew, P. Pownraj, S. Abdulla, B. Pullithadathil, Technologies for clinical diagnosis using expired human breath analysis. Diagnostics 5 (2015) 27-60.

[25] C. Chen, M. Jiang, X. Luo, H. Tai, Y. Jiang, M. Yang, Y. Su, Ni-Co-P hollow nanobricks enabled humidity sensor for respiratory analysis and human-machine interfacing. SENSOR ACTUAT B-CHEM 370 (2022) 132441.
[26] T. Pan, Z. Yu, F. Huang, H. Yao, G. Hu, C. Tang, J. Gu, Flexible Humidity Sensor with High Sensitivity and Durability for Respiratory Monitoring Using Near-Field Electrohydrodynamic Direct-Writing Method. ACS Appl. Mater. Interfaces 15 (2023) 28248-28257.
[27] N. Wang, J. Tong, J. Wang, Q. Wang, S. Chen, B. Sheng, Polyimide-Sputtered and Polymerized Films with Ultrahigh Moisture Sensitivity for Respiratory Monitoring and Contactless Sensing. ACS Appl. Mater. Interfaces 14 (2022) 11842-11853.
[28] M. Yan, Q. Hao, S. Diao, F. Zhou, C. Yichen, N. Jiang, C. Zhao, X. R. Ren, F. Yu, J. Tong, D. Wang, H. Liu, Smart Home Sleep Respiratory Monitoring System Based on a Breath-Responsive Covalent Organic Framework. ACS nano 18 (2024) 728-737.
[29] J. Guo, K. Zhang, R. Dai, M. Nie, Y. Li, Q. Wang, Flexible Sensor for Invisible Respiratory Monitoring via Construction of a 2D Stacked Micronetwork. ACS omega 5 (2020) 32806-32813.
[30] Y. Gu, J. Hao, T. Wu, Z. Zhang, Z. Zhang, Q. Li, Bimetallic MoNi/WNi nanoalloys for ultra-sensitive wearable temperature sensors. J. Mater. Chem. A 10 (2022) 5402-5409.
[31] Y. Wang, Y. Hong, X. Hu, Y. Ye, P. Wang, J. Luo, J. Wei, Flexible Fabric Temperature Sensor Based on Vo2/Pedot: Pss with High Performance. Adv. Mater. Technol. 8 (2023) 2300898.
[32] L. Jin, Y. Zheng, Z. Liu, J. Li, H. Zhai, Z. Chen, Y. Li, Design of an Ultrasensitive Flexible Bend Sensor Using a Silver-Doped Oriented Poly (vinylidene fluoride) Nanofiber Web for Respiratory Monitoring. ACS Appl. Mater. Interfaces 12 (2020) 1359-1367.
[33] A. Kumar, K. R. K. Rakesh, M. O. Shaikh, C. H. Lu, J. Y. Yang, H. L. Chang, C. H. Chuang, Ultrasensitive Strain Sensor Utilizing a AgF–AgNW Hybrid Nanocomposite for Breath Monitoring and Pulmonary Function Analysis. ACS Appl. Mater. Interfaces 14 (2022) 55402-55413.
[34] C. Ning, R. Cheng, Y. Jiang, F. Sheng, J. Yi, S. Shen, Y. Zhang, X. Peng, K. Dong, Z. L. Wang, Helical Fiber Strain Sensors Based on Triboelectric Nanogenerators for Self-Powered Human Respiratory Monitoring. ACS nano 16 (2022) 2811-2821.
[35] J. Huang, G. Xie, Q. Wei, Y. Su, X. Xu, Y. Jiang, Degradable MXene-Doped Polylactic Acid Textiles for Wearable Biomonitoring. ACS Appl. Mater. Interfaces 15 (2022) 5600-5607.
[36] H. Pan, G. Chen, Y. Chen, A. C. Di, M. A. Mayer, S. Shen, J. Chen, Biodegradable cotton fiber-based piezoresistive textiles for wearable biomonitoring. BIOSENS BIOELECTRON 222 (2023) 114999.
[37] Q. Wei, G. Chen, H. Pan, Z. Ye, C. Au, C. Chen, J. Chen, MXene-sponge based high-performance piezoresistive sensor for wearable biomonitoring and real-time tactile sensing. Small Methods 6 (2022) 2101051.
[38] G. Chen, R. Guan, M. Shi, X. Dai, H. Li, N. Zhou, H. Mao, A nanoforest-based humidity sensor for respiration monitoring. Microsyst. Nanoeng. 8 (2022) 44.
[39] Q. Zhang, G. Xie, M. Duan, Y. Liu, Y. Cai, M. Xu, Y. Su, Zinc oxide nanorods for light-activated gas sensing and photocatalytic applications. ACS Appl. Nano Mater. 6 (2023) 17445-17456.
[40] Q. Zhang, C. Chen, Y. Liu, M. Xu, G. Xie, H. Tai, Y. Su, Room-temperature light-activated chemical sensors for gas monitoring and applications: a review. J PHYS D APPL PHYS 55 (2022) 213001.
[41] M. Yang, C. Au, G. Deng, S. Mathur, Q. Huang, X. Luo, J. Chen, NiWO4 microflowers on multi-walled carbon nanotubes for high-performance NH3 detection. ACS Appl. Mater. Interfaces 13 (2021) 52850-52860.
[42] S. Sharma, A. Thapa, S. Singh, T. Mondal, Crosstalk-free graphene-liquid elastomer based printed sensors for unobtrusive respiratory monitoring. NANOSCALE 16 (2024) 3498-359.
[43] J. Li, G. Xie, J. Jiang, Y. Liu, C. Chen, W. Li, Y. Su, Enhancing photodegradation of Methyl Orange

by coupling piezo-phototronic effect and localized surface plasmon resonance. Nano Energy 108 (2023) 108234.
[44] H. Guan, R. Yang, W. Li, Y. Tao, C. Chen, H. Tai, W. Li, Self-powered multifunctional flexible sensor for wearable biomonitoring. SENSOR ACTUAT B-CHEM 377 (2023) 132996.
[45] W. Li, T. Yang, C. Liu, Y. Huang, C. Chen, H. Pan, Z. Hong, Optimizing piezoelectric nanocomposites by high-throughput phase-field simulation and machine learning. Adv. Sci. 9 (2022) 2105550.
[46] Y. Chen, W. Li, C. Chen, H. Tai, G. Xie, Y. Jiang, Y. Su, Perspectives on self-powered respiration sensor based on triboelectric nanogenerator. Appl. Phys. Lett. 119 (2021).
[47] Y. Su, M. Yao, G. Xie, H. Pan, H. Yuan, M. Yang, Y. Jiang, Improving sensitivity of self-powered room temperature NO2 sensor by triboelectric-photoelectric coupling effect. Appl. Phys. Lett. 115 (2019).
[48] X. Song, M. Tang, C. Wang, X. Li, J. Zhu, J. Shao, S. Huang, B. Wang, X. P. Li, H. Li, H. Xu, Stereocomplexation-Enhanced Electroactivity of Poly (lactic acid) Nanofibrous Membranes for Long-Term PM Capturing and Remote Respiratory Monitoring. ACS Sustainable Chem. Eng. 12 (2024) 3554-3564.
[49] M. Wang, J. Zhang, Y. Tang, J. Li, B. Zhang, E. Liang, Y. Mao, X. Wang, Air-Flow-Driven Triboelectric Nanogenerators for Self-Powered Real-Time Respiratory Monitoring. ACS nano 12 (2018) 6156-6162.
[50] Q. Xu, X. Gao, S. Zhao, Y. N. Liu, D. Zhang, K. Zhou, H. Khanbareh, W. Chen, Y. Zhang, C. Bowen, Construction of Bio-Piezoelectric Platforms: From Structures and Synthesis to Applications. Adv. Mater. 33 (2021) 2008452.
[51] S. Zhang, M. Bick, X. Xiao, G. Chen, A. Nashalian, J. Chen, Leveraging triboelectric nanogenerators for bioengineering. Matter 4 (2021) 845-887.
[52] G. Chen, X. Zhao, S. Andalib, J. Xu, Y. Zhou, T. Tat, J. Chen, Discovering giant magnetoelasticity in soft matter for electronic textiles. Matter 4 (2021) 3725-3740.
[53] Y. Fang, J. Xu, X. Xiao, Y. Zou, X. Zhao, Y. Zhou, J. Chen, A deep-learning-assisted on-mask sensor network for adaptive respiratory monitoring. Adv. Mater. 34 (2022) 2200252.
[54] Q. Li, C. Ding, W. Yuan, R. Xie, X. Zhou, Y. Zhao, Z. Liu, Highly stretchable and permeable conductors based on shrinkable electrospun fiber mats. Adv. Fiber Mater. 3 (2021) 302-311.
[55] S. Bhattacharya, I. Roy, A. Tice, C. Chapman, R. Udangawa, V. Chakrapani, R. J. Linhardt, High-conductivity and high-capacitance electrospun fibers for supercapacitor applications. ACS Appl. Mater. Interfaces 12 (2020) 19369-19376.
[56] H. Chang, S. Kim, S. Jin, S. W. Lee, G. T. Yang, K. Y. Lee, H. Yi, Ultrasensitive and Highly Stable Resistive Pressure Sensors with Biomaterial-Incorporated Interfacial Layers for Wearable Health-Monitoring and Human–Machine Interfaces. ACS Appl. Mater. Interfaces 10 (2018) 1067-1076.
[57] M. H. Islam, S. Afroj, M. A. Uddin, D. V. Andreeva, K. S. Novoselov, N. Karim, Graphene and CNT-based smart fiber-reinforced composites: a review. Adv. Funct. Mater. 32 (2022) 2205723.
[58] Y. Wu, S. Tan, G. Fang, Y. Zhang, G. Ji, Manipulating CNT Films with Atomic Precision for Absorption Effectiveness–Enhanced Electromagnetic Interference Shielding and Adaptive Infrared Camouflage. Adv. Funct. Mater. (2024) 2402193.
[59] J. Zhu, B. Deng, J. Yang, D. Gang, Modifying activated carbon with hybrid ligands for enhancing aqueous mercury removal. CARBON 47 (2009) 2014-2025.
[60] D. E. Newbury, N. W. M. Ritchie, Performing elemental microanalysis with high accuracy and high precision by scanning electron microscopy/silicon drift detector energy-dispersive X-ray spectrometry (SEM/SDD-EDS). J. Mater. Sci. 50 (2015) 493-518.
[61] H. P. Karki, L. Kafle, D. P. Ojha, J. H. Song, H. J. Kim, Cellulose/Polyacrylonitrile Electrospun Composite Fiber for Effective Separation of the Surfactant-Free Oil-in-Water Mixture under a Versatile Condition. Sep. Purif. Technol. 210 (2018) 913-919.
[62] M. H. M. Facure, L. A. Mercante, D. S. Correa, Polyacrylonitrile/Reduced Graphene Oxide Free-

Standing Nanofibrous Membranes for Detecting Endocrine Disruptors. ACS Appl. Nano Mater. 5 (2022) 6376-6384.
[63] S. Murugesan, K. Myers, V. Subramanian, Amino-functionalized and acid treated multi-walled carbon nanotubes as supports for electrochemical oxidation of formic acid. Appl. Catal. B Environ. 103 (2011) 266-274.
[64] H. Kong, Z. Song, W. Li, Y. Bao, D. Qu, Y. Ma, Z. Liu, W. Wang, Z. Wang, D. Han, L. Niu, Skin-Inspired Hair–Epidermis–Dermis Hierarchical Structures for Electronic Skin Sensors with High Sensitivity over a Wide Linear Range. ACS nano 15 (2021) 16218-16227.
[65] D. Geng, S. Chen, R. Chen, Y. You, C. Xiao, C. Bai, W. Zhou, Tunable wide range and high sensitivity flexible pressure sensors with ordered multilevel microstructures. Adv. Mater. Technol. 7 (2022) 2101031.
[66] S. K. Illi, U. Held, I. Frank, C. M. Spengler, Effect of respiratory muscle training on exercise performance in healthy individuals: a systematic review and meta-analysis. SPORTS MED 42 (2012) 707-724.
[67] E. Tharion, P. Samuel, R. Rajalakshmi, G. Gnanasenthil, R. K. Subramanian, Influence of deep breathing exercise on spontaneous respiratory rate and heart rate variability: a randomised controlled trial in healthy subjects. Indian J Physiol Pharmacol 56 (2012) 80-87.
[68] G. Chen, S. Shen, T. Tat, X. Zhao, Y. Zhou, Y. Fang, J. Chen, Wearable respiratory sensors for COVID-19 monitoring. VIEW 3 (2022) 20220024.

Declaration of interests

☒ The authors declare that they have no known competing financial interests or personal relationships that could have appeared to influence the work reported in this paper.

☐ The author is an Editorial Board Member/Editor-in-Chief/Associate Editor/Guest Editor for [*this journal* (Journal Name)] and was not involved in the editorial review or the decision to publish this article.

☐The authors declare the following financial interests/personal relationships which may be considered as potential competing interests:

Highlights

●A hierarchical CNT@PAN smart textile was constructed for biomonitoring

●The latex encapsulation enables moist and thermal stability.

●A rapid response/recovery time of 192/104 ms was achieved.

●Versatile breathing patterns and respiratory diseases can be discerned.